

Intermediate-wavelength cyclotron waves in simple metals and Fermi-liquid effects

G. L. Dunifer

*Department of Physics, Wayne State University, Detroit, Michigan 48202
and Bell Laboratories, Murray Hill, New Jersey 07974*

P. H. Schmidt and W. M. Walsh, Jr.

Bell Laboratories, Murray Hill, New Jersey 07974

(Received 15 November 1976; revised manuscript received 22 November 1978)

In this paper we explore the propagation of cyclotron waves of intermediate wavelength in a simple metal with a spherical Fermi surface. We show experimentally how thick plates of potassium metal can be used to study the lowest branch of the multivalued dispersion relation and to find the locations of turning points on the dispersion curve. The methods employed allow the dispersion curve to be studied at relatively large wave vectors, a region in which the Fermi-liquid parameter A_1 can produce observable modifications. Although the present experiments agree well with a free-electron model, we present numerical calculations showing the effects of A_1 and A_2 on the dispersion curve and note in particular the circumstances under which one should be able to determine A_1 experimentally.

I. INTRODUCTION

Under the conditions of low temperature and an applied magnetic field, a pure metal can support several modes of propagating electromagnetic waves.^{1,2} One example is that of cyclotron waves,³ which propagate perpendicular to the magnetic field in the vicinity of the fundamental Azbel-Kaner (AK) cyclotron resonance and each of its subharmonics. These waves have generally been referred to as long wavelength, intermediate wavelength, or short wavelength, according to whether $qR \ll 1$, $qR \approx 1$, or $qR \gg 1$, respectively, where q is the wave vector of the excitation and $R = v_F/\omega$ is the cyclotron radius at cyclotron resonance. Although seen in a variety of metals,⁴⁻⁶ the cyclotron waves have been studied most extensively in the alkali metals,^{3,7-10} primarily in the long-wavelength limit.

In this paper we are concerned with intermediate-wavelength cyclotron waves in the alkali-metal potassium. We present experimental data obtained with a technique⁵ that locates the turning points¹¹ of the dispersion relation, making it possible to follow the waves to much shorter wavelengths than before. In the long-wavelength regime the dispersion characteristics of the wave are affected by the Landau Fermi-liquid parameters^{3,12} A_2 , A_3 , A_4, \dots , and experimental studies in this regime have determined approximate numbers for some of these parameters in the alkali metals.^{3,7-9} Although neither A_0 nor A_1 influence the dispersion of the waves in the long-wavelength limit, we show by numerical calculation how A_1 can have an influence in the intermediate-wavelength regime. In particular, we show how our present experimental techniques may be used to deter-

mine the parameter A_1 with the proper choice of frequency.

II. PHYSICAL CHARACTERISTICS OF CYCLOTRON WAVES

Cyclotron wave propagation occurs under the same experimental conditions as those required for observation of well-resolved AK cyclotron-resonance spectra: i.e., samples of high purity at low temperature with sufficiently high excitation frequencies that $\omega\tau \gg 1$, where τ is the average electron scattering time due to lattice imperfections. The characteristics of the waves are given by their dispersion relation, for whose calculation we choose a coordinate system with z axis parallel to the applied magnetic field \vec{H} and x axis parallel to the wave vector of the excitation \vec{q} . Maxwell's equations yield two dispersion relations corresponding to two distinct types of cyclotron waves: the ordinary and the extraordinary modes. The ordinary mode is a purely transverse wave in which $\vec{E}_{\text{tr}} \parallel \vec{H}$; the extraordinary mode contains a mixture of transverse and longitudinal components in which $\vec{E}_{\text{tr}} \perp \vec{H}$. Neglecting the displacement current in comparison to the conduction current, the dispersion relations can be written in the following dimensionless forms³:

$$(qR)^2 = [(\omega_p/\omega)v_F/c]^2 i\omega\tau\sigma_{zz}/\sigma_0 \quad (1)$$

for the ordinary wave, and

$$(qR)^2 = [(\omega_p/\omega)v_F/c]^2 i\omega\tau/\sigma_0(\sigma_{yy} + \sigma_{xy}^2/\sigma_{xx}) \quad (2)$$

for the extraordinary mode, where ω is the frequency of the wave, ω_p is the plasma frequency, v_F is the Fermi velocity, c is the speed of light, σ_0 is the dc electrical conductivity in zero mag-

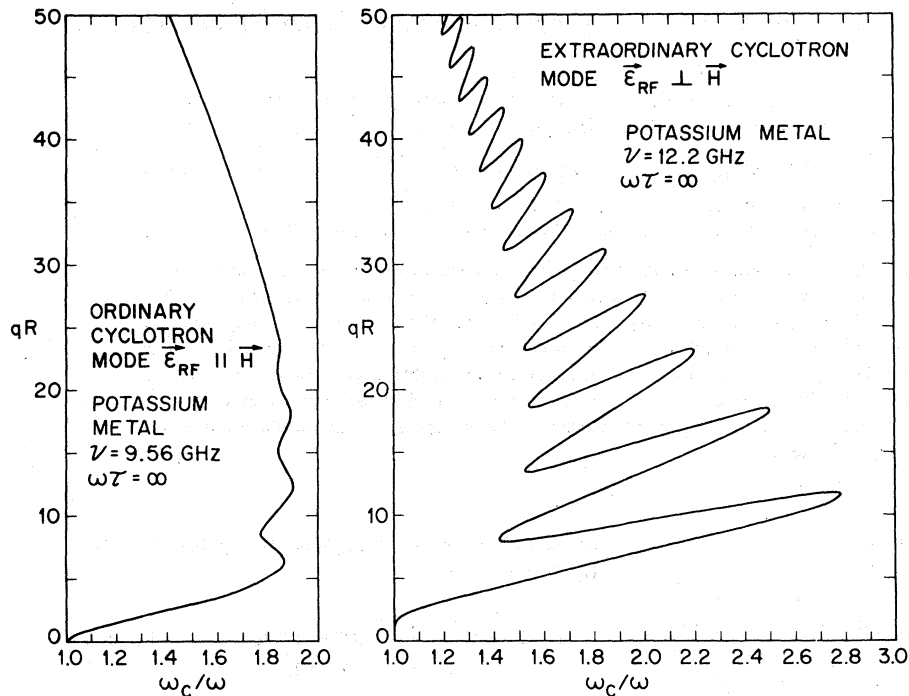


FIG. 1. Example of the free-electron cyclotron wave dispersion relations for the ordinary and the extraordinary modes associated with the fundamental AK cyclotron resonance.

netic field, and σ_{ij} are the components of the frequency-, wave-vector-, and magnetic-field-dependent magnetoconductivity tensor.

Figure 1 is a numerical evaluation of Eqs. (1) and (2) showing far into the intermediate-wavelength regime the ordinary and extraordinary modes associated with the fundamental AK cyclotron resonance. The plots are made in terms of the dimensionless quantities qR and ω_c/ω . This type of plot is most suitable for comparison with the experimental data, for which the applied frequency ω is held constant while the cyclotron frequency ω_c is continually varied as the magnetic field is swept. The frequencies chosen lie within the X-band microwave frequency range, and the parameters used are those for potassium metal with the exception of τ , which was taken as infinite in order to suppress the damping of the waves. Both modes begin at $\omega_c/\omega = 1$ for zero wave vector, extend to higher magnetic fields for increasing wave vector, develop oscillations in the intermediate-wavelength regime, and then return asymptotically to $\omega_c/\omega = 1$ in the short-wavelength regime ($qR \gg 1$). The oscillations associated with the extraordinary mode are appreciably stronger than those of the ordinary mode and are the ones whose turning points show up most clearly in our data. The set of turning points lying at the higher magnetic fields will be classified as the outer turning points, and that set lying at the lower magnetic fields will be classified as the inner turning points. Thus, when the magnetic field (or ω_c/ω)

is being increased, the crossing of an inner turning point "turns on" the propagation of two more cyclotron waves of slightly different wavelength, while the crossing of an outer turning point "turns off" the propagation of two cyclotron waves. The turning points are labeled as first, second, third, . . . , etc., starting at the smallest qR value and progressing to increasing values of qR .

In the free-electron limit the ordinary mode occurs as a single mode at the fundamental AK cyclotron resonance and each of its subharmonics. The extraordinary mode, however, occurs as a single mode only at the fundamental resonance and becomes a double mode at each of the subharmonics.¹¹ Figure 2 illustrates the two extraordinary modes associated with the first subharmonic of AK cyclotron resonance. The two modes are classified as the ω^+ and the ω^- modes. Although both are mixtures of transverse and longitudinal components, the ω^+ modes become primarily transverse waves at large qR while the ω^- modes become primarily longitudinal waves in the same limit. In the limit of short wavelength ($qR \gg 1$), the ω^+ modes return asymptotically to the same values of ω_c/ω at which they originated, whereas the ω^- modes asymptotically approach those values of ω_c/ω associated with the adjacent subharmonic on the high field side. The turning points of the ω^+ and ω^- modes on the subharmonics are too close together in magnetic field to be resolved individually in our data. However, we show in Sec. IV how they influence the surface impe-

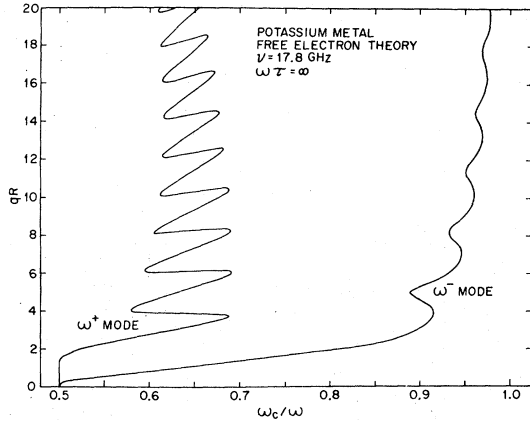


FIG. 2. Free-electron dispersion relations for the two extraordinary modes associated with the first sub-harmonic of AK cyclotron resonance.

dance of our samples.

An important property of the cyclotron waves is the manner in which they are influenced by Fermi-liquid or many-body effects. Azbel¹³ has shown that in the short-wavelength regime many-body effects have no influence. On the other hand, as mentioned previously, all the Landau Fermi-liquid parameters with the exception of A_0 and A_1 appear in the dispersion curves in the long-wavelength limit. A_0 and A_1 are unimportant because of the very high plasma frequency of the conduction electrons in a typical metal, $\omega_p \approx 10^{16} \text{ sec}^{-1}$. From the Landau-Silin transport equation it is seen that A_0 is associated with any net charge density produced by a disturbance and that A_1 is associated with any net current flow that may take place. Because the experiments are typically performed at microwave frequencies much below the plasma frequency, the waves at long wavelength are characterized by both zero charge fluctuations and zero current flow; consequently A_0 and A_1 do not occur in the dispersion relation in this limit. The nature of the disappearance of A_1 at long-wavelengths can be seen from the dispersion relation itself, which in its most general form can be written

$$(qR)^2 = [(\omega_p/\omega)v_F/c]^2 f(qR, \omega_c/\omega), \quad (3)$$

where $f(qR, \omega_c/\omega)$ is a function only of qR and ω_c/ω and is made up of the same set of conductivity components as indicated in Eqs. (1) and (2). At small wave vector both $(qR)^2$ and $f(qR, \omega_c/\omega)$ are ≈ 1 , whereas the coefficient $(\omega_p v_F/\omega c)^2$ is $\approx 10^5$ at X-band frequencies. Consequently, under these conditions the dispersion relation is quite accurately written $f(qR, \omega_c/\omega) = 0$. For both the ordinary and the extraordinary modes, however, f is composed of just the proper combination of

conductivity components, which when set equal to zero automatically sets the net current equal to zero also.

In order for A_1 to become important the two sides of Eq. (3) must be comparable. This requires relatively large-wavevector and high-frequency excitations. Since $f \approx 1/qR$ at large wave vector, Eq. (3) requires

$$qR \gtrsim [(\omega_p/\omega)v_F/c]^{2/3}. \quad (4)$$

For potassium metal at X-band frequencies this gives $qR \approx 50$, which is not much greater than the maximum wave vector resolved in the data we present. From Eq. (4) it is also clear that there must be a frequency below which A_1 cannot modify the dispersion relation at any wave vector, i.e., that frequency for which Eq. (4) is not satisfied before entering the short-wavelength regime. Conversely, as the excitation frequency is raised, the effects of A_1 will become apparent, and the higher the frequencies employed the smaller the wave vector at which A_1 can influence the dispersion relation. Although the frequencies used in obtaining our present data are not high enough to exhibit any appreciable modifications by A_1 , we present numerical computations showing at what frequencies such modifications will occur and what the nature of such modifications will be, and, most important, we demonstrate the experimental techniques that will be necessary at these higher frequencies.

In order to compare the data with theory, we will use a method previously employed,³ which avoids solving the complete boundary-value problem. The exact solution is extremely difficult to obtain because the coupling to the cyclotron waves is so strong that the problem must be treated self-consistently. Although it still remains unsolved, a theoretical discussion of the present status of the boundary-value problem is given by Fredkin and Wilson.¹⁴ Instead we solve for the infinite-medium dispersion relation and attempt to correlate it with features seen in the experimental data obtained from a finite metal slab. This appears to be a fairly realistic approach as one is dealing primarily with wave propagation in the bulk of the metal as both the wavelength and sample thickness are orders of magnitude larger than the anomalous skin depth in which the waves are excited. The excellent agreement between the data and the infinite-medium dispersion curves attests to the validity of this approach.

III. EXPERIMENTAL TECHNIQUES

There are two ways in which cyclotron wave propagation can be studied with a single microwave

cavity. In one method³ the samples are fabricated into thin plates, which are placed into a microwave cavity in such a fashion that the rf electric fields present can induce electrical currents to flow on *both* faces of the sample simultaneously. Under the appropriate conditions of magnetic field strength these linearly polarized surface currents give rise to cyclotron waves propagating from the surfaces into the bulk of the sample. When the samples are made thin enough that transmission of the cyclotron waves through the sample can take place, oscillations in the surface impedance are observed as the magnetic field is swept. These oscillations of the power absorption result from the varying phase of the transmitted currents relative to the primary driving currents present at each surface. In the second method⁵ samples sufficiently thick to suppress all transmission are used, and one observes certain anomalies in the surface impedance at particular magnetic fields. These anomalies arise from the turning points of the dispersion relation at intermediate wavelengths and are due to the "turning on" or "turning off" of certain cyclotron waves at the turning points, as discussed earlier. These anomalies thus provide a way for studying the dispersion relation into the intermediate-wavelength regime, a region in which the transmission method produces rather-complex interference spectra^{9,15} due to the simultaneous propagation of waves of several different wavelengths.

Most of the samples studied in this investigation were fabricated with thickness sufficiently large ($L \approx 0.6$ – 0.8 mm) so as to attenuate all propagating excitations. A small number, however, were made slightly thinner ($L \approx 0.5$ mm), which leads to the complete attenuation of all propagating cyclotron waves with the exception of the longest wavelength branch. This branch, which is the most slowly attenuated, can then be studied to appreciably higher values of wave vector and magnetic field, into regions where interference patterns are observed for thinner samples.

The experiments used ultrahigh-purity potassium obtained by high-vacuum distillation at pressures $\approx 10^{-8}$ Torr. Resistivity ratios $\rho(295 \text{ K})/\rho(1.4 \text{ K})$ in the range 15 000–18 000 for the bulk material were obtained. The samples were fabricated in a dry box containing a high-purity argon atmosphere in which the total amounts of oxygen, nitrogen, and water vapor were maintained at less than 1 ppm by volume. The potassium was first extruded in the form of a thick polycrystalline ribbon by a hydraulic press.¹⁶ For about half of the samples the ribbon was then permanently pressed between two thin glass plates, forming samples that, when placed into a microwave cavity, were

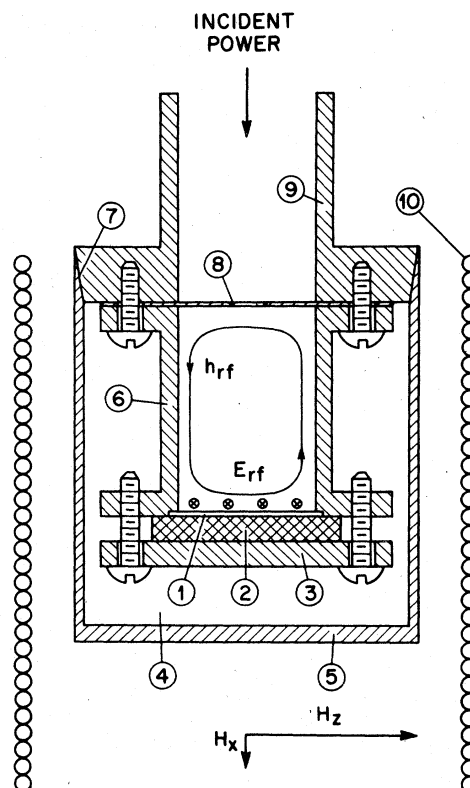


FIG. 3. Simplified view of the microwave cavity and that type of sample which makes up the end wall of the cavity. Omitted from the figure are the Dewar system and the cryogenic liquids surrounding the vacuum can. Indicated in the figure are: 1. Glass plate or window. 2. Potassium sample. 3. Brass end plate. 4. Helium exchange gas. 5. Vacuum can. 6. Microwave cavity. 7. Grease seal between vacuum can and the waveguide flange. 8. Coupling iris. 9. Waveguide. 10. Water-cooled solenoid coaxial with the waveguide for generating the H_x field perpendicular to the plane of the sample.

excited on both surfaces by the rf electromagnetic fields. For the remaining samples the potassium ribbon was fabricated into the end wall of the microwave cavity, as indicated in Fig. 3. In this case, only one glass window was used and only one surface of the sample was exposed to the incident microwave power. In both cases the use of glass plates resulted in very smooth and flat surfaces that had brilliant, mirrorlike appearances.

Figure 3 illustrates the geometrical arrangement of the sample with respect to the rectangular microwave cavity and the rf and dc fields present. The dc magnetic field is composed of two components: H_z , lying approximately in the plane of the sample and produced by a 15-in. Varian electromagnet (capacity of 25 kG); and H_x , situated approximately perpendicular to the plane of the

sample and produced by a small water-cooled solenoid (capacity of 600 G) wound around the tail of the Dewar between the poles of the Varian magnet. By accurately adjusting the relative strengths of H_x and H_z , the field can be very accurately aligned parallel to the surface of the sample. The H_z field can be rotated in the plane of the sample for alignment either parallel or perpendicular to the microwave electric field \vec{E}_H to couple to the ordinary or extraordinary modes, respectively.

As shown, the cavity is situated in a vacuum can with thermal contact to a surrounding liquid-helium bath provided by a small amount of helium exchange gas in the can. The temperature of the samples was varied over the range 1.4–4.2 K by pumping on the liquid helium.

The experiments were performed at three distinct microwave frequencies: 12.2, 17.8, and 34.6 GHz. The changes in the surface impedance of the sample were monitored in reflection by a conventional homodyne bridge spectrometer. The bridge was balanced to detect changes in the real part of the surface impedance of the sample—the surface resistance. By employing field-modulation and phase-sensitive detection, the field derivative of the surface resistance dR/dH was recorded as a function of the magnetic field.

IV. EXPERIMENTAL RESULTS

We begin first with the thickest samples, which display semi-infinite behavior in the sense that all propagating modes are completely attenuated before passing through the sample. Figure 4(a) displays the derivative spectrum of such a sample for the extraordinary mode geometry at a frequency of 12.2 GHz and a temperature of 1.5 K. The spectrum is dominated by a series of AK-cyclotron-resonance single-particle resonance peaks occurring at $\omega_c/\omega = 1/n$, $n = 1, 2, 3, \dots$, for which the cyclotron frequency $\omega_c = eH/m^*c$ is determined by an isotropic effective mass $m^* = 1.21m_0$.¹⁷ The fundamental resonance and first few subharmonics show a slight splitting, which may reflect a lack of perfect sample flatness or possibly the onset of cyclotron wave propagation. The splitting grows very rapidly, dominating the spectrum, for rotations of the magnetic field out of the plane of the sample by less than 2° . Even with the field aligned absolutely parallel to the surface a residual amount of splitting (as shown) remains for all the samples studied.

In Fig. 4(b) an increase in gain by a factor of 10 over the range $1.5 \leq \omega_c/\omega \leq 3.5$ displays a sharp dip and a series of seven peaks, the latter lying on a rising background. These features we attribute to the anomalies in the surface resistance

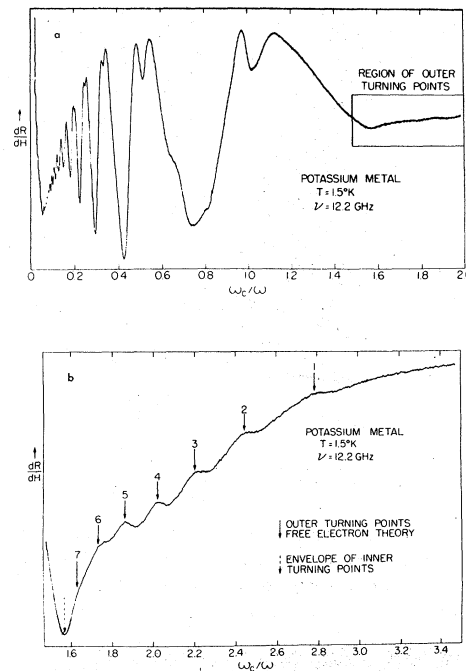


FIG. 4. (a) AK cyclotron-resonance derivative spectra in the extraordinary-mode polarization. (b) Same as (a) with the gain increased by 10 to display the turning point anomalies. The arrows are at the locations of the turning point singularities of the free-electron, infinite- $\omega\tau$ dispersion relation.

caused by turning points in the cyclotron wave dispersion curve. The solid arrows in the figure correspond to the first seven outer turning points of the infinite- $\omega\tau$ free-electron dispersion relation. Within the experimental accuracy to which they can be determined ($\omega_c/\omega = \pm 0.005$), the locations of the seven peaks coincide exactly with the locations of the theoretical turning points. We thus empirically identify the peaks in dR/dH with the outer turning points of the dispersion relation. This identification proves valid in that increasing the frequency to 17.8 GHz and then further to 34.6 GHz causes shifts in the observed resistance anomalies, which are again exactly matched (within $\omega_c/\omega = \pm 0.005$) by the appropriate dispersion curves. With increasing temperature the peaks broaden, but *do not shift in position*, thus making appropriate our comparison with the infinite- $\omega\tau$ dispersion curves.

An inspection of Fig. 1 shows that the seventh outer turning point occurs at $qR \approx 37$, well into the region where the orbit diameters of the electrons exceed the wavelength of the wave. It is also clear why outer turning points of still higher qR values are not readily seen—they lie much closer together in magnetic field and also begin to overlap the locations of the inner turning points. The

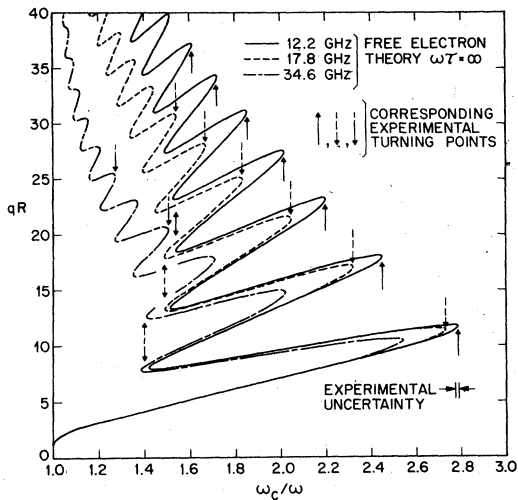


FIG. 5. Free-electron dispersion relations for the extraordinary mode cyclotron wave at 12.2, 17.8, and 34.6 GHz. The arrows locate the experimental peaks and dips in dR/dH at each frequency.

inner turning points are also situated very close together in field and consequently cannot be individually resolved. We note, however, that the sharp dip in dR/dH preceding the seven outer turning point anomalies of Fig. 4(b) lies exactly at the high-field edge of the envelope of inner turning points (where their density is highest). Once again this identification proves empirically valid in that similar sharp dips in dR/dH occur at exactly the same high-field edge of the inner turning point envelope at our two higher frequencies.

We are unable to advance any physical arguments as to why the onset of wave propagation at the inner turning points and the cessation of wave propagation at the outer turning points should result in dips and peaks in dR/dH , respectively. Gordon and Frandsen²¹ have evaluated the surface impedance for a spherical Fermi surface in the approximation of pseudospecular reflection, but the position, shape, and intensity of their anomalies do not agree with our own observations. For present purposes, therefore, we will use the empirical identification as a means of mapping the intermediate-wavelength behavior of the cyclotron waves.

Figure 5 shows the theoretical dispersion curves for the three frequencies at which our data were taken. The curves display an appreciable frequency dependence, especially at the higher wave vectors. Also indicated by arrows are the experimental turning points as determined empirically by peaks and dips in dR/dH . Within experimental uncertainties the correspondence between the free-electron theory and the data are exact at all

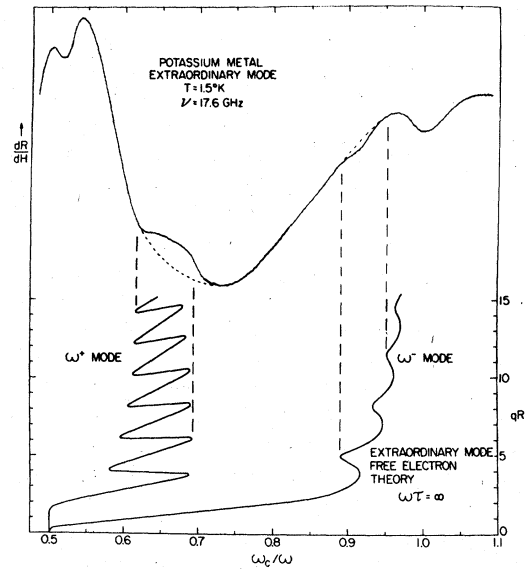


FIG. 6. Experimental trace taken in the extraordinary wave geometry between the fundamental and first subharmonic of AK cyclotron resonance, showing anomalies associated with the ω^+ and the ω^- modes. The lower portion of the figure indicates the dispersion relations of the two modes and the correlation between the observed anomalies and the locations of the theoretical turning points.

three frequencies and at all wave vectors for which anomalies have been detected. The high-field edge of the envelope of the inner turning points shows up as a dip at each frequency, and at both 12.2 and 17.8 GHz all turning points at higher fields than this dip are detected. At 34.6 GHz we are not able to sweep the magnetic field into the range of the first three outer turning points. We do, however, detect the fourth and the sixth outer turning points at this frequency. The fifth turning point is presumably obscured by its proximity in field to the third of the inner turning points.

Figure 6 displays anomalies in the surface resistance due to the turning points of the ω^+ and the ω^- modes associated with the first subharmonic of AK cyclotron resonance. For the subharmonic waves the turning points are too close together to be individually resolved in our present experiments. The effect of their presence, nevertheless, can be seen from the figure. For the ω^+ mode a rather strong anomaly occurs, beginning at the high-field limit of the inner turning points and extending to the high-field limit of the outer turning points. The ω^- mode produces an appreciably weaker anomaly situated between the first and third inner turning points, that region in which the oscillations are strongest. Anomalies due to the ω^+ modes are observed down to the

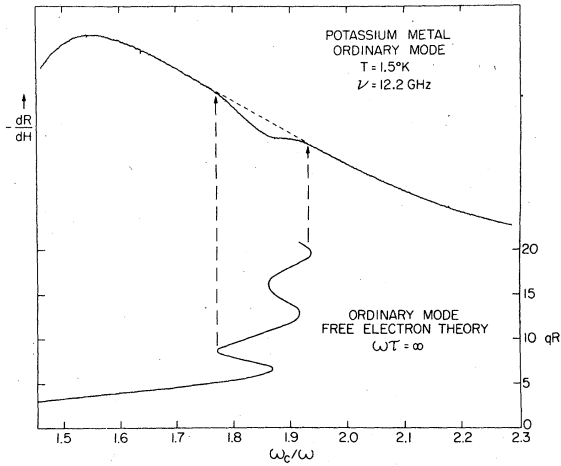


FIG. 7. Experimental trace taken in the ordinary wave geometry showing the anomaly in the surface resistance arising from oscillations in the dispersion curve of the fundamental cyclotron wave.

fourth subharmonic, whereas anomalies due to the ω^- modes have been observed only on the first two subharmonics.

In Fig. 7 the dc magnetic field has been rotated 90° in the plane of the sample to couple to the ordinary mode. The ordinary mode has only a few turning points and they are very close together, as indicated in Figs. 1 and 7. Again, an anomaly arising from the oscillations in the dispersion relation is seen beginning at the first inner turning point and extending to the third outer turning point, the high-field limit of the oscillations.

We next consider samples that are somewhat thinner ($L \approx 0.5$ mm) than those previously discussed. Figure 8 illustrates the extraordinary dispersion relation when a finite scattering time τ is included in Eq. (2). When τ is finite and is treated as a real quantity, the solution for the wave vector q becomes complex, with the real part of q describing the propagation characteristics of the wave and the imaginary part of q describing the damping or attenuation of the wave.^{18,19} Parts (a) and (b) of the figure indicate, respectively, the real and imaginary parts of q . In Fig. 8(a) we see that for finite values of τ the previously continuous dispersion curve splits up into a series of discrete branches that no longer join together. The linear portions of the infinite- $\omega\tau$ curve (between the oscillations) are little affected by finite values of $\omega\tau$. The major modifications come near the turning points and beyond in the previously forbidden region where propagation did not occur for infinite $\omega\tau$. Figure 8(b) indicates the damping of the wave with each curve corresponding to one of the branches of the real part of the dispersion relations. Higher damping is associated with an in-

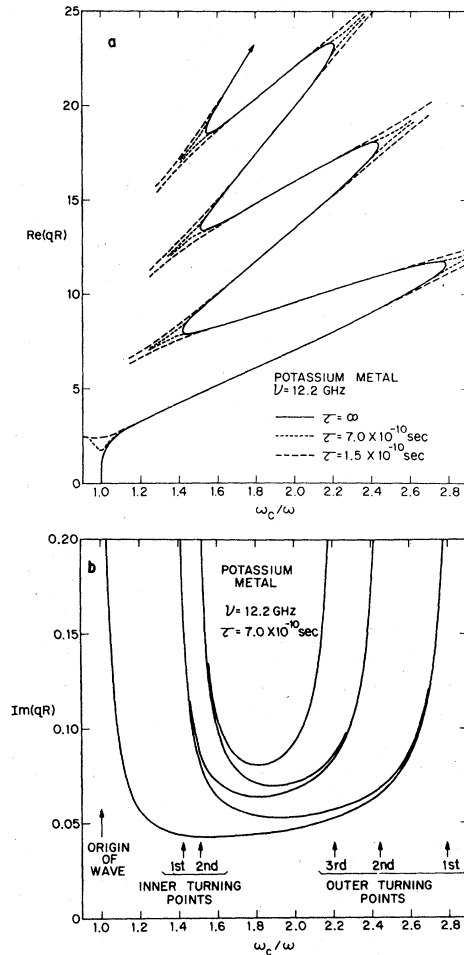


FIG. 8. Extraordinary-wave free-electron dispersion relations for finite values of $\omega\tau$. (a) The real part of the dispersion relation describing the propagation of the wave for three values of τ . (b) The imaginary part of the dispersion relation describing the attenuation and damping of the wave. Each curve corresponds to one of the branches indicated in (a) with the larger values of $\text{Im}(qR)$ associated with the larger values of $\text{Re}(qR)$.

crease in the imaginary part of q with signal intensity $\approx \exp[-\text{Im}(q)L]$, where L is the sample thickness. It is seen that the damping becomes very large in the vicinity of the turning points. Even though a wave can actually propagate beyond a turning point of the infinite- $\omega\tau$ dispersion relation, it becomes very strongly damped in this region. Minimum damping occurs between the turning points in the linear portion of the real part of the curve. Although the turning points actually disappear for finite values of $\omega\tau$, we note experimentally that the anomalies in the surface resistance still exist and that decreasing $\omega\tau$ only broadens and weakens the anomalies but does not shift their location in magnetic field from their infinite-

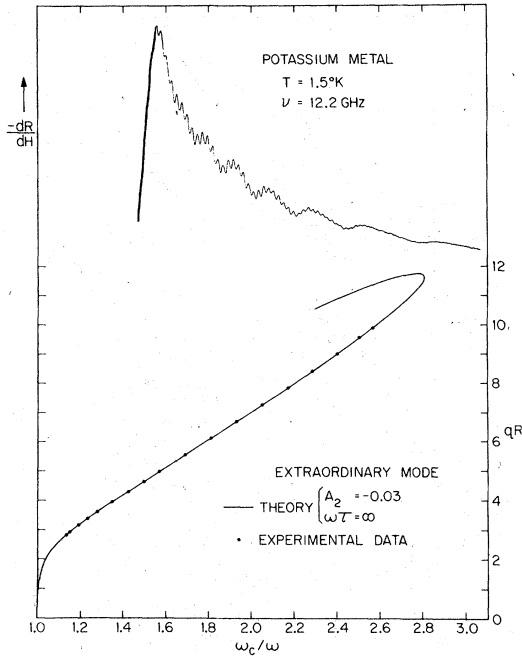


FIG. 9. Derivative spectra for a somewhat thinner sample ($L = 0.51$ mm) showing the transmission of the first branch of the dispersion curve superimposed on the surface resistance anomalies. The lower part of the figure compares the transmission spectra with the infinite- $\omega\tau$ dispersion curve for $A_2 = -0.03$.

$\omega\tau$ positions. Frandsen and Gordon^{20,21} have recently stressed the important modifications that finite- $\omega\tau$ can introduce into the dispersion curve. Although this is true in general, our observations indicate that the locations of the turning point anomalies are independent of $\omega\tau$ and that only their widths and strengths are affected.

An important feature of Fig. 8 is that as the real part of q increases so does the imaginary part. This means that the higher qR branches of the dispersion relation are more strongly attenuated than the smaller qR branches. In previous studies of the extraordinary mode⁸ relatively thin samples were used, and as a consequence once the magnetic field was increased beyond the first inner turning point, a rather-complicated interference pattern between several propagating waves resulted. Figure 8 suggests that by choosing the proper thickness of the sample carefully, one should be able to attenuate all branches of the dispersion curve below experimental detectability except for the first or lowest qR branch. By so doing one would be able to observe the first branch to appreciably higher values of ω_c/ω and qR than possible in thin plates.

In the top part of Fig. 9 are plotted experimental data in the vicinity of the outer turning points for a potassium sample whose thickness was carefully

chosen in the manner just described ($L = 0.51$ mm). In addition to the turning-point anomalies, we see superimposed a rather-high-frequency oscillation that results from the transmission of the first-branch cyclotron wave through the sample. As described previously this oscillation is due to the varying phase of the transmitted current beating with the primary driving currents present at each surface of the sample. Each oscillation corresponds to an increase of 1 in the total number of wavelengths contained within the sample. From the position in field and the total number of oscillations present one can plot out an experimental dispersion curve to be compared with theory.³ Such a comparison is made in the lower part of Fig. 9. The infinite- $\omega\tau$ dispersion relation is plotted for $A_2 = -0.03$. In the central portion of the curve only every fifth oscillation is plotted. As can be seen, we obtain an excellent agreement between experiment and theory. Although using $A_2 = -0.03$ in the theory gives an improved fit over the free electron theory, this comparison is not a sensitive test for determining A_2 as A_2 only weakly affects this particular mode for small wave vector.³ With the use of thick samples we are able to follow the first branch of the dispersion curve up to $\omega_c/\omega = 2.6$ and $qR = 10$ in comparison to the limits of $\omega_c/\omega = 1.4$ and $qR = 4$ obtained with thin samples. For the particular sample shown in Fig. 9 the largest wave-vector transmission signal that can be detected corresponds to a total number of 93 (l) wavelengths included within the sample.

Figure 10 illustrates the temperature dependence of these signals for the sample of Fig. 9. Note the increase in gain by a factor of 2.5 at the two highest temperatures. As can be seen both the transmission signals and the surface resistance anomalies depend strongly on the temperature. The transmission oscillations are strongest at 1.4 K and have essentially disappeared by 4.2 K. The surface resistance anomalies also decrease rapidly in amplitude with increasing temperature. Although the overall baseline and the widths of the anomalies change with temperature, note that the locations of the peaks is temperature independent.

V. THEORY AND NUMERICAL COMPUTATIONS

We have seen how surface resistance anomalies in thick samples give a method of studying portions of the dispersion relation (the turning points) to fairly large values of qR where the Fermi-liquid parameter A_1 can have an influence. Our present experiments, although demonstrating the necessary experimental techniques, have so far shown excellent agreement with the free-electron theory. In order to determine when A_1 will produce an

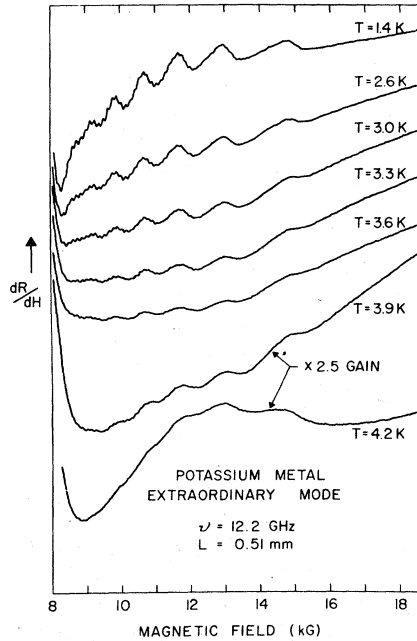


FIG. 10. Temperature dependence of the cyclotron wave transmission and surface resistance anomalies. The gain at the two highest temperatures has been increased by a factor of 2.5.

observable effect and what influence it will have, we now begin a numerical computation of the theoretical dispersion relation.

The dispersion curves shown in the previous figures, plus the ones to follow, were all calculated from Eqs. (1) and (2). These equations are exact except for the omission of the displacement current, which is completely negligible at microwave frequencies. The presence of Fermi-liquid effects modifies the components of the conductivity tensor that go into the two equations. For numerical evaluation of the equations we use the algorithms of Fredkin and Wilson¹⁴ as formulated in the Appendix.

The two numerical quantities needed to describe the potassium samples are ω_p and v_F . To obtain the plasma frequency we use

$$\omega_p = (4\pi N e^2 / m^*)^{1/2}. \quad (5)$$

The number of conduction electrons per unit volume $N = 1.398 \times 10^{22} \text{ cm}^{-3}$ is obtained by the lattice spacing at 1.5 K: $a = 5.2295 \text{ \AA}$,²² assuming one conduction electron per atom. The effective mass $m^* = 1.21m_0$ is obtained from AK cyclotron-resonance data.²³ Using these numbers in Eq. (5) we obtain $\omega_p = 6.065 \times 10^{15} \text{ sec}^{-1}$. To obtain the Fermi velocity we use

$$m^* v_F = \hbar k_F^0 = \hbar k_F^0, \quad (6)$$

where k_F^0 is the Fermi wave vector calculated in

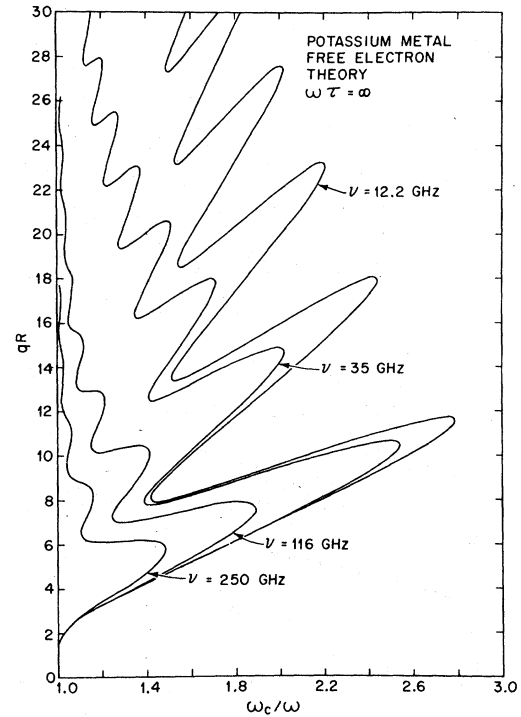


FIG. 11. Frequency dependence of the free-electron extraordinary-mode dispersion relation for the cyclotron wave associated with the fundamental AK cyclotron resonance.

the free-electron limit from the density of the conduction electrons. Equation (6) follows from the known sphericity of the Fermi surface²⁴ and the invariance of the volume of the Fermi surface in the presence of Fermi-liquid interactions.²⁵ Making use of

$$k_F^0 = (3\pi^2 N)^{1/3} = 0.7450 \times 10^8 \text{ cm}^{-1} \quad (7)$$

we obtain $v_F = 0.7128 \times 10^8 \text{ cm/sec}$. This gives us at 12.2 GHz, for example, $(\omega_p v_F / \omega c)^2 = 3.539 \times 10^4$.

Figure 11 displays the frequency dependence of the free-electron extraordinary mode dispersion relation for that cyclotron wave associated with the fundamental AK cyclotron resonance. With increasing frequency the curves are pushed to smaller values of magnetic field (ω_c/ω). This frequency dependence is a direct result of finite electrical current flow. As long as the $(qR)^2$ term in Eq. (2) remains negligible in comparison to the right-hand side of the equation, there is no appreciable current flow and the dispersion relation is a universal function of qR and ω_c/ω , showing no frequency dependence. As $(qR)^2$ becomes comparable with the other term, an electrical current begins and the dispersion relation becomes frequency dependent. The fact that the dispersion curves in Fig. 5 show an appreciable dependence

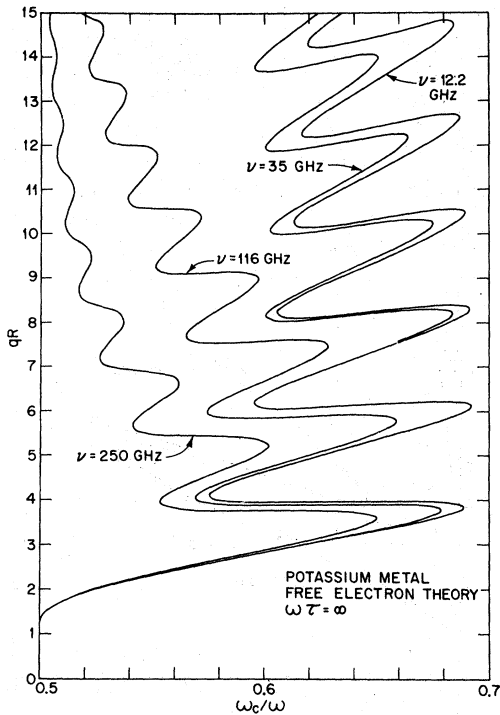


FIG. 12. Frequency dependence of the free-electron ω^+ mode dispersion relation for the cyclotron wave associated with the first subharmonic of AK cyclotron resonance.

on the frequency of the cyclotron wave indicates that even at those frequencies and wave vectors we are entering the regime in which current flow takes place and A_1 can modify the dispersion of the wave.

Figure 12 shows the frequency dependence of the ω^+ mode associated with the first subharmonic of AK cyclotron resonance. Once again the curves are pushed to lower values of magnetic field with increasing ω , although the frequency dependence is not as strong as it was for the fundamental wave. The ω^- modes turn out to be completely independent of the applied frequency. The ω^- mode for the first subharmonic displayed in Fig. 2 is thus valid for all frequencies (much less than the plasma frequency).

Figure 13 indicates the effect that a finite value of A_1 has on the fundamental cyclotron wave at the relatively high frequencies of 116 and 250 GHz. The values $A_1 = \pm 0.2$ have approximately 2–4 times the magnitude expected for potassium metal from detailed many-body calculations.^{26,27} As seen, a negative value of A_1 pushes the turning points to higher values of ω_c/ω while a positive value of A_1 pushes them to lower ω_c/ω . At 116 GHz the maximum shift is 1.3% in field and occurs at the third outer turning point. At 250 GHz the maximum shift is 2.4% in field and occurs at the second

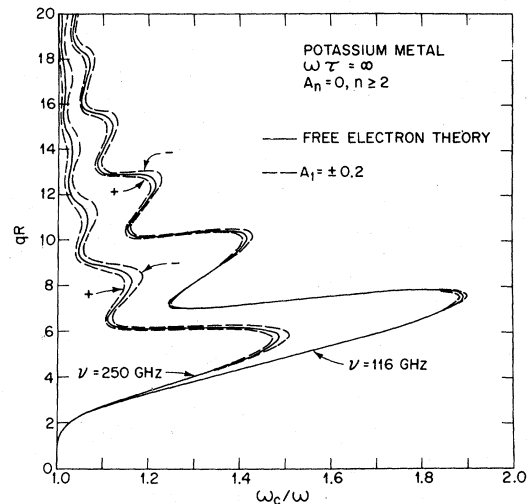


FIG. 13. Cyclotron wave dispersion curve displaying the effects of A_1 on the extraordinary mode at frequencies of 116 and 250 GHz.

outer turning point. Therefore, as expected, the modifications introduced by A_1 are larger and occur at smaller wavevectors with increasing frequency.

In Fig. 14 we show how the parameter A_2 affects the same dispersion relation. Again the value of A_2 used in the plot is several times larger than

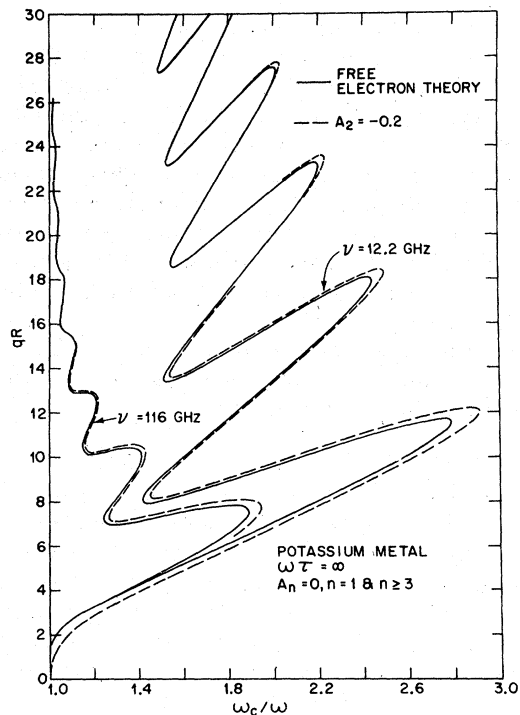


FIG. 14. Cyclotron wave dispersion curve displaying the effects of A_2 on the extraordinary mode at frequencies of 12.2 and 116 GHz.

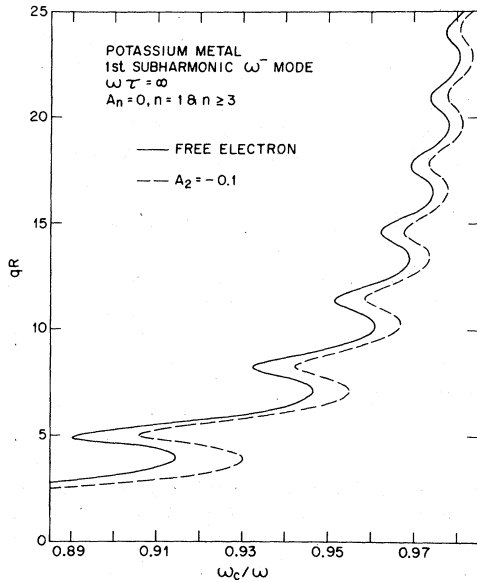


FIG. 15. Cyclotron wave dispersion curve displaying the effects of A_2 on the ω^- mode associated with the first subharmonic of AK cyclotron resonance.

the value measured experimentally ($A_2 \approx -0.03$). The effects of A_2 are quite different. Although a negative value of A_2 again pushes the turning points out to higher magnetic field, the shifts continuously decrease with the increasing wavevector and become smaller as the frequency is increased. This means the effects of A_2 can be easily separated from those of A_1 . In fact, at the frequencies necessary to determine A_1 the effects of the known value of A_2 will be completely negligible in comparison.

The effects of the Fermi-liquid parameters A_1 and A_2 on the subharmonics has been studied only on the first subharmonic waves because of the large amount of computer time required to do the calculations. For the ω^+ mode A_1 has the same type of effect as it did on the fundamental wave except the shifts are about ten times smaller in field and occur at appreciably larger wave vectors. The shifts caused by A_2 are again similar to those on the fundamental wave but once more several times smaller in size. The ω^- mode is completely unaffected by the parameter A_1 . The effect of A_2 on this mode is shown in Fig. 15.

VI. CONCLUSION

We have seen how the dispersion relation of the extraordinary mode cyclotron waves can be studied at intermediate wavelengths by observing surface impedance anomalies associated with the turning points of the dispersion curves. If the expected values of A_1 and A_2 for potassium metal are used

in the calculations of the dispersion relations, the deviations from the free electron turning points are less than the uncertainties of our experimental measurements—in agreement with our excellent fit to the free electron theory. We have shown by numerical computation, however, that the same type of experimental observations carried out at frequencies ≥ 200 GHz should allow a determination of the Fermi-liquid parameter A_1 .

ACKNOWLEDGMENTS

Helpful conversations with P. M. Platzman, T. M. Rice, and E-Ni Foo are gratefully acknowledged. We should especially like to thank D. R. Fredkin and A. R. Wilson for sharing their algorithms with us before publication. The technical assistance of L. W. Rupp with the computer runs and that of M. R. Pattison in the preparation of the figures are appreciated. Research at Wayne State University was supported in part by the NSF under Grant No. DMR 72-00181 AO1. Portions of the manuscript were prepared with the facilities of the Department of Physics, Imperial College of Science and Technology, London.

APPENDIX

The algorithms of Fredkin and Wilson,¹⁴ used for calculating the dispersion relations in the presence of Fermi-liquid effects, have been set up as follows. For the ordinary wave Eq. (1) can be written

$$(qR)^2 = -[(\omega_p/\omega)v_F/c]^2 G_{10}, \quad (A1)$$

where G_{10} is to be obtained from the simultaneous solution of the $\frac{1}{2}L_{\max}(L_{\max}+1)$ equations

$$G_{1m} - \sum_{l'm'} K_{lm'}^{l'm'} \frac{A_{l'}}{1+A_{l'}} G_{l'm'} = K_{lm}^{10}. \quad (A2)$$

L_{\max} is the highest order A_l parameter to be retained; l and l' range from 1 to L_{\max} ; for each l value m ranges from $-l$ to $+l$; and for each l' value m' ranges from $-l'$ to $+l'$. In Eq. (A2) only those terms are retained for which both $l-m$ and $l'-m'$ are odd:

$$K_{lm}^{l'm'} = 2\pi^2 \left(\frac{\omega}{\omega_c}\right) (-1)^{m<} \\ \times \int_0^\pi \sin\theta d\theta \frac{J_{y+m>}(x) J_{-(y+m<)}(x)}{\sin(\pi y)} \\ \times C_{lm}(\theta) C_{l'm'}(\theta), \quad (A3)$$

where $y = (\omega + i/\tau)/\omega_c$; $x = (qR)(\omega/\omega_c) \sin\theta$; $m_{<}$ = algebraically smaller of m and m' ; $m_{>}$ = algebraically larger of m and m' ; $J_y(x)$ = ordinary Bessel function of the first kind; $C_{lm}(\theta) = e^{-im\phi} Y_{lm}(\theta, \phi)$; Y_{lm} are the spherical harmonics of Condon and

Shortley²⁸; θ = integration variable. For the extraordinary mode Eq. (2) can be written in the form

$$(qR)^2 = 2 \left(\frac{\omega_p}{\omega} \frac{v_F}{c} \right)^2 \left(\frac{G_{11}^1 G_{1-1}^{-1} - G_{1-1}^1 G_{11}^{-1}}{G_{11}^1 + G_{11}^{-1} - G_{1-1}^1 - G_{1-1}^{-1}} \right), \quad (\text{A4})$$

where $G_{l\pm 1}^\mu$ ($\mu = \pm 1$) is to be obtained from the $\frac{1}{2}(L_{\max} + 1)(L_{\max} + 2)$ equations

$$G_{l'm}^\mu - \sum_{l''m''} K_{l'm}^{l''m''} \frac{A_{l''}}{1 + A_{l''}} G_{l''m''}^\mu = \mu K_{l'm}^{1-\mu}. \quad (\text{A5})$$

L_{\max} , l , l' , m , and m' are defined as before and

vary over the same ranges, except in Eq. (A5) only those terms are retained in which both $l - m$ and $l' - m'$ are even. $K_{l'm}^{l''m''}$ is again defined as in Eq. (A3).

The integration over θ in Eq. (A3) is done numerically to an accuracy of 1 part in 10^4 using Simpson's rule, and the system of equations listed in Eqs. (A2) or (A5) is solved in matrix form on a computer. For finite $\omega\tau$ the solutions for q become complex with the imaginary part of q resulting in the damping of the wave as discussed previously.

¹E. A. Kaner and V. G. Skobov, *Adv. Phys.* **17**, 605 (1968).

²P. M. Platzman and P. A. Wolff, *Waves and Interactions in Solid State Plasmas*, Supplement No. 13 (Academic, London, 1973).

³P. M. Platzman, W. M. Walsh, Jr., and E-Ni Foo, *Phys. Rev.* **172**, 689 (1968).

⁴V. S. Edel'man, *Sov. Phys.-JETP Lett.* **9**, 177 (1969).

⁵J. O. Henningsen, *J. Low Temp. Phys.* **4**, 163 (1971).

⁶Cyclotron Waves in high-purity copper crystals have been observed by S. Schultz and co-workers (private communication).

⁷D. Pinkel, G. L. Dunifer, and S. Schultz (unpublished).

⁸W. M. Walsh, Jr., P. M. Platzman, P. S. Percy, L. W. Rupp, Jr., and P. H. Schmidt, *Proceedings of the Twelfth International Conference on Low Temperature Physics, Kyoto, 1970* (Keigaku, Tokyo, 1971).

⁹W. M. Walsh, Jr., and P. M. Platzman, *Proceedings of the Tenth International Conference on Low Temperature Physics, Moscow, 1966* (VINITI, Moscow, 1967).

¹⁰G. L. Dunifer, P. H. Schmidt, and W. M. Walsh, Jr., *Phys. Rev. Lett.* **26**, 1553 (1971).

¹¹E-Ni Foo, *Phys. Rev.* **182**, 674 (1969).

¹²The Fermi-liquid parameters A_l are defined according to the convention in Ref. 3 and can be expressed as $A_l/(2l+1)$ in terms of the Fermi-liquid parameters sometimes used by other authors.

¹³M. Ya Azbel', *Sov. Phys.-JETP* **7**, 527 (1958).

¹⁴D. R. Fredkin and A. R. Wilson (unpublished).

¹⁵K. Saermark and J. Lebeck, *Phys. Status Solidi B* **65**, 543 (1974).

¹⁶Sample fabrication techniques used in this investiga-

tion are described more completely in G. L. Dunifer, D. Pinkel, and S. Schultz, *Phys. Rev. B* **10**, 3159 (1974).

¹⁷C. C. Grimes and A. F. Kip, *Phys. Rev.* **132**, 1991 (1963).

¹⁸J. B. Frandsen, L. E. Hasselberg, J. Lebeck, and K. Saermark, *Phys. Status Solidi B* **67**, 501 (1975).

¹⁹J. B. Frandsen, *Proc. LT-14 Conf.* **4**, 321 (1975).

²⁰J. B. Frandsen and R. A. Gordon, *Phys. Rev. B* **14**, 4342 (1976).

²¹R. A. Gordon and J. B. Frandsen, *Solid State Commun.* **24**, 221 (1977).

²²S. A. Werner, E. Gurmon, and A. Arrott, *Phys. Rev.* **186**, 705 (1969).

²³As reported more recently by W. M. Walsh, Jr., L. W. Rupp, Jr., P. H. Schmidt, and R. N. Castellano, *Bull. Am. Phys. Soc.* **18**, 336 (1973), higher-frequency spectra may lead to a slight revision in the value of m^* . Precision measurements of the onset of cyclotron wave propagation for the second- and highest-order subharmonics of AK cyclotron resonance lead to a self-consistent mass $m^*/m_0 = 1.217 \pm 0.002$ and a revised value $A_2 = -0.022 \pm 0.002$.

²⁴D. Shoenberg and P. J. Stiles, *Proc. R. Soc. (London)* **A 281**, 62 (1964).

²⁵J. M. Luttinger, *Phys. Rev.* **119**, 1153 (1960).

²⁶T. M. Rice, *Phys. Rev.* **175**, 858 (1968).

²⁷T. M. Rice (private communication).

²⁸E. U. Condon and G. H. Shortley, *Theory of Atomic Spectra* (Cambridge University, Cambridge, England, 1963).